



Providing Choice & Value
Generic CT and MRI Contrast Agents



CONTACT REP

AJNR

This information is current as
of July 30, 2025.

Virtual Monoenergetic Images from Spectral Detector CT Enable Radiation Dose Reduction in Unenhanced Cranial CT

R.P. Reimer, D. Flatten, T. Lichtenstein, D. Zopfs, V.
Neuhaus, C. Kabbasch, D. Maintz, J. Borggreffe and N.
Große Hokamp

AJNR Am J Neuroradiol 2019, 40 (10) 1617-1623
doi: <https://doi.org/10.3174/ajnr.A6220>
<http://www.ajnr.org/content/40/10/1617>

Virtual Monoenergetic Images from Spectral Detector CT Enable Radiation Dose Reduction in Unenhanced Cranial CT

R.P. Reimer, D. Flatten, T. Lichtenstein, D. Zopfs, V. Neuhaus, C. Kabbasch, D. Maintz, J. Borggrefe, and N. Große Hokamp

ABSTRACT

BACKGROUND AND PURPOSE: Our aim was to evaluate whether improved gray-white matter differentiation in cranial CT by means of 65-keV virtual monoenergetic images enables a radiation dose reduction compared to conventional images.

MATERIALS AND METHODS: One hundred forty consecutive patients undergoing 171 spectral detector CTs of the head between February and November 2017 (56 ± 19 years of age; male/female ratio, 56%/44%) were retrospectively included. The tube current-time product was reduced during the study period, resulting in 61, 55, and 55 patients being examined with 320, 290, and 260 mAs, respectively. All other scanning parameters were kept identical. The volume CT dose index was recorded. ROIs were placed in gray and white matter on conventional images and copied to identical positions in 65-keV virtual monoenergetic images. The contrast-to-noise ratio was calculated. Two radiologists blinded to the reconstruction technique evaluated image quality on a 5-point Likert-scale. Statistical assessment was performed using ANOVA and Wilcoxon test adjusted for multiple comparisons.

RESULTS: The mean volume CT dose index was 55, 49.8, and 44.7 mGy using 320, 290, and 260 mAs, respectively. Irrespective of the volume CT dose index, noise was significantly lower in 65-keV virtual monoenergetic images compared with conventional images (65-keV virtual monoenergetic images/conventional images: extraocular muscle with 49.8 mGy, $3.7 \pm 1.3/5.6 \pm 1.6$ HU, $P < .001$). Noise slightly increased with a reduced radiation dose (eg, extraocular muscle in conventional images: $5.3 \pm 1.4/5.6 \pm 1.6/6.1 \pm 2.1$ HU). Overall, the contrast-to-noise ratio in 65-keV virtual monoenergetic images was superior to that in conventional images irrespective of the volume CT dose index ($P < .001$). Particularly, 65-keV virtual monoenergetic images with 44.7 mGy showed significantly lower noise and a higher contrast-to-noise ratio than conventional images with 55 mGy ($P < .001$). Subjective analysis confirmed better image quality in 65-keV virtual monoenergetic images, even using 44.7 mGy.

CONCLUSIONS: The 65-keV virtual monoenergetic images from spectral detector CT allow radiation dose reduction in cranial CT. While this proof of concept included a radiation dose reduction of 19%, our data suggest that even greater reduction appears achievable.

ABBREVIATIONS: CI = conventional images; CNR = contrast-to-noise ratio; CTDI_{vol} = volume CT dose index; VMI = virtual monoenergetic images

Unenhanced cranial CT is the standard examination for patients with acute neurologic deficits to allow fast diagnosis of emergencies, for instance, intracranial hemorrhage or ischemia.¹⁻⁴ There are approximately 70 million cranial CT scans annually in the United States alone; out of these, several scans are performed in the same patient, so that they undergo

repetitive scanning.⁵ Despite rapid advances in the field of CT imaging such as dose modulation or iterative image reconstruction, few of these have been applied to cranial CT for 2 main reasons: First, there are only subtle differences in attenuation between gray and white matter. Yet, this is one of the most important aspects to evaluate, in particular in light of suspected ischemia. Second, the surrounding skull causes beam-hardening and therefore an increase in image noise due to beam-hardening.⁶⁻⁹ Hence, possibilities for dose reduction are limited, despite radiosensitive tissues such as the eye lenses being exposed.¹⁰⁻¹³

A recent development in the field of CT is dual-energy CT, which has been evolving for the past decade. Dual-energy CT is known to improve soft-tissue contrast by means of virtual monoenergetic images (VMI).¹⁴⁻¹⁶ These VMI further reduce artifacts

Received May 17, 2019; accepted after revision August 5.

From the Department of Diagnostic and Interventional Radiology, University of Cologne, Faculty of Medicine and University Hospital Cologne, Cologne, Germany. R.P. Reimer and D. Flatten contributed equally to this work.

Please address correspondence to Nils Große Hokamp, MD, Department of Diagnostic and Interventional Radiology, University Hospital Cologne, Cologne, Germany, Kerpener Str 62, 50937 Köln, Germany; e-mail: nils.grosse-hokamp@uk-koeln.de

<http://dx.doi.org/10.3174/ajnr.A6220>

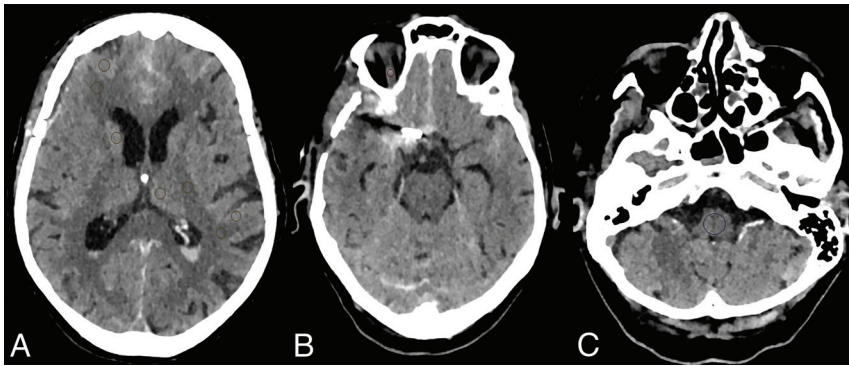


FIG 1. ROI placement in the cortical gray and juxtacortical white matter, in the thalamic parenchyma and posterior limb of the internal capsule, in the caudate nucleus (*orange ROIs*), in an extraocular muscle (*red ROI*), and in the medulla oblongata (*blue ROI*) on an axial plane showing the basal ganglia (A), the orbital cavity (B), and the posterior fossa (C).

occurring due to beam-hardening. In light of neuroimaging, dual-energy CT demonstrated improved image quality and lesion characterization, while it also allowed material separation for iodine.^{15,17-22}

Dual-energy CT systems register low- and high-energy data attenuation profiles. By linear blending of these datasets, VMI can be reconstructed. VMI represent virtually approximated images, which would result from acquisition with a true monoenergetic x-ray beam. They are typically available in a range from 40 to 200 keV, depending on the dual-energy CT system used.^{23,24}

Different emission-based dual-energy CT systems have been available for several years using emission spectra with lower and higher mean energy.^{25,26} More recently, a detector-based approach was introduced, referred to as spectral detector CT. Here, low- and high-energy photons are registered separately using a dual-layer detector.^{24,26} The upper layer is yttrium-based and registers lower energy photons, while the lower layer is gadolinium oxysulfide-based, registering higher energy photons.^{8,24,26}

In a recent study, VMI from spectral detector CT showed superior image quality in examinations of the head compared with conventional images (CI). Corticomedullary differentiation was found to be best in 65-keV VMI (VMI_{65keV}), while in lower kiloelectron volt images, beam-hardening artifacts close to the calvaria distorted image quality.⁶ Their data suggest a VMI-enabled radiation dose reduction.

Therefore, the aim of our study was to compare VMI_{65keV} with CI from unenhanced spectral detector CT datasets of the head acquired with different acquisition protocols to evaluate whether improved image quality in VMI_{65keV} allows a reduction of radiation dose.

MATERIALS AND METHODS

To meet national requirements for radiation dose, we modified protocols for cranial CT examinations, including a reduction in the radiation dose. The institutional review board later approved the scientific evaluation of these data and waived informed consent due to the retrospective study design. A structured search in the radiology information system was performed with the following inclusion criteria: 1) older than 18 years of age, 2) an unenhanced spectral detector CT of the head between the February 1,

2017, and November 30, 2017, and 3) a standardized imaging protocol as described below. Exclusion criteria were the following: 1) extensive intracranial hemorrhage or edema, 2) craniectomy or hemicraniectomy, and 3) artifacts due to patient movement or implants. Eventually, 140 patients with 171 CT scans were included in this study.

Acquisition Parameters

All CT scans were performed for clinical indications on the same spectral detector CT scanner (IQon Spectral CT; Philips Healthcare, Best, the Netherlands). Sixty-one of the identified

CT scans were obtained with a tube current-time product of 320 mAs, 55 with 290 mAs, and 55 with 260 mAs. All other scan parameters were kept identical: tube voltage = 120 kV (peak), pitch = 0.36, rotation time = 0.33 seconds, and collimation = 64 × 0.625. CI were reconstructed using a hybrid iterative reconstruction algorithm (iDose4, Filter UB; Philips Healthcare). VMI_{65keV} were reconstructed using a dedicated spectral image-reconstruction algorithm (Spectral, Filter UB; Philips Healthcare). Denoising for both was set to a medium level (level 3 of 7). All images were reconstructed with a section thickness of 1 mm and a section increment of 1 mm.

Dose-length product and volume CT dose index (CTDI_{vol}) were recorded from the radiation dose report. We further compared the anterior-posterior and lateral dimensions of the head between groups to exclude this as a confounder.

Quantitative Analysis

Quantitative analysis was performed using ROI-based measurements of attenuation and SD in the following areas on a representative axial plane: 1) cortical gray and 2) adjacent juxtacortical white matter of the frontal and parietal lobes, 3) thalamic parenchyma, 4) adjacent posterior limb of the internal capsule, 5) caudate nucleus, 6) extraocular muscle, and 7) medulla oblongata (Fig 1).

ROIs were placed on CI and copied to identical positions in VMI_{65keV}. The size of the ROIs was kept constant at 25 mm², except for the ROI in the medulla oblongata (100 mm²), and was only adjusted to avoid inclusion of unrepresentative tissue. One radiologist with 2 years of experience in cranial CT interpretation performed the quantitative analysis. In a randomly chosen subgroup of 30 cranial CT scans, a second reader repeated the ROI placement to assess interrater reliability.

Image noise was considered as an SD of extraocular muscle. The contrast-to-noise ratio (CNR) of the gray and white matter of the frontal and parietal lobes was calculated as the difference of the average Hounsfield unit, divided by the square root of the sum of the SD of the 2 adjacent ROIs.^{6,15}

Qualitative Analysis

Qualitative analysis was performed independently by 2 fellowship-trained trained neuroradiologists. Readers were blinded to

the reconstruction technique. Rating was performed on 5-point Likert scales with regard to assessment of gray-white matter differentiation in the following areas: 1) the basal ganglia, 2) the supratentorial cortex, 3) the infratentorial cortex, and 4) the subcalvarial space (1 = not diagnostic; 2 = severely impaired assessment; 3 = moderate assessment; 4 = fair assessment; 5 = good assessment, fully diagnostic). Furthermore, visually perceived image noise and beam-hardening artifacts in the subcalvarial space were evaluated (1 = excessive; 2 = severe; 3 = moderate; 4 = some; 5 = no visually perceptible noise).

Statistical Analysis

All analyses were performed using JMP Software (Version 12; SAS Institute, Cary, North Carolina) unless specified below. To compare groups, we used ANOVA or Wilcoxon tests, adjusted for multiple comparisons if appropriate. A *P* value < .05 was considered significant. Results are shown as mean ± SD. Interrater reliability was determined by means of intraclass correlation estimates using R Studio (Version 1.1.456; <http://rstudio.org/download/desktop>) based on a single rater, consistency, 2-way mixed-effects model for the quantitative analysis and based on a mean of 2 raters, consistency, 2-way mixed-effects model for the qualitative analysis.²⁷ Interrater agreement was evaluated as described earlier: excellent (intraclass correlation coefficient > 0.8), good (intraclass correlation coefficient > 0.6), moderate (intraclass correlation coefficient > 0.4), and poor agreement (intraclass correlation coefficient ≤ 0.4).^{28,29}

Table 1: Radiation dose

Tube Current–Time Product (mAs)	320	290	260
DLP (mGy × cm) ^a	1014.9 ± 56.9	937.7 ± 40.2	837.7 ± 45.6
Radiation dose reduction		−7.6%	−17.5%
CTDI _{vol} (mGy)	55	49.8	44.7
Radiation dose reduction		−9.5%	−18.7%

Note:—DLP indicates dose-length product.

^aResults are means ± SDs.

Table 2: Quantitative results of attenuation, noise, and CNR^a

CTDI _{vol} (mGy)	CI			VMI _{65keV}		
	55	49.8	44.7	55	49.8	44.7
Attenuation						
GM	34.0 ± 1.4	33.4 ± 1.5	34.1 ± 1.7	34.6 ± 1.3	34.2 ± 1.2	35.1 ± 1.5
WM	26.5 ± 1.2	26.1 ± 1.5	27.0 ± 1.6	26.4 ± 1.1	26.0 ± 1.3	27.1 ± 1.4
Thalamus	33.6 ± 1.5	33.2 ± 1.6	34.4 ± 1.9	34.4 ± 1.4	33.9 ± 1.4	35.5 ± 1.8
Posterior limb	26.5 ± 2.2	26.3 ± 2.0	26.6 ± 2.2	26.1 ± 1.4	26.0 ± 1.7	26.6 ± 2.0
Caudate nucleus	34.5 ± 4.4	35.2 ± 2.1	35.4 ± 2.3	35.7 ± 1.5	35.8 ± 1.8	36.3 ± 2.1
Extraocular muscle	32.8 ± 5.6	31.1 ± 6.4	33.2 ± 8.1	31.9 ± 5.6	30.8 ± 6.2	35.4 ± 9.9
Medulla oblongata	31.5 ± 4.3	32.0 ± 4.5	34.6 ± 4.9	31.1 ± 3.3	31.0 ± 3.0	33.9 ± 3.7
Noise						
GM	4.5 ± 0.8	4.6 ± 0.7	4.8 ± 0.8	3.1 ± 0.6	3.1 ± 0.5	3.2 ± 0.5
WM	4.5 ± 0.7	4.8 ± 0.8	4.9 ± 0.7	3.0 ± 0.5	3.2 ± 0.5	3.3 ± 0.6
Thalamus	5.8 ± 0.8	6.0 ± 1.0	6.1 ± 1.1	4.0 ± 0.7	4.2 ± 0.8	4.3 ± 0.9
Posterior limb	5.2 ± 1.0	5.5 ± 1.1	5.6 ± 1.3	3.6 ± 0.8	3.7 ± 0.9	3.9 ± 1.0
Caudate nucleus	5.4 ± 1.1	5.6 ± 1.2	5.6 ± 0.8	3.7 ± 0.9	3.8 ± 0.8	3.8 ± 0.6
Extraocular muscle	5.3 ± 1.4	5.6 ± 1.6	6.1 ± 2.1	3.6 ± 1.1	3.7 ± 1.3	4.2 ± 1.6
Medulla oblongata	6.1 ± 1.2	6.4 ± 1.2	6.7 ± 1.4	4.4 ± 1.0	4.6 ± 0.9	4.7 ± 0.9
GM-WM CNR	2.5 ± 0.5	2.4 ± 0.5	2.3 ± 0.5	3.4 ± 0.5	3.3 ± 0.5	3.2 ± 0.5

^aResults are means ± SDs.

RESULTS

The mean age of patients was 55.8 ± 18.6 years; of these patients, 61 (43.6%) were women and 79 (56.4%) men.

Radiation Dose

CTDI_{vol} was 55, 49.8, and 44.7 mGy in examinations with 320, 290, and 260 mAs, respectively. The dose-length product was 1014.9 ± 56.9, 937.7 ± 40.2, and 837.7 ± 45.6 mGy × cm (*P* < .001) (Table 1). Regarding the CTDI_{vol}, the radiation dose was reduced by 9.5% and 18.7%. No significant differences in head size between groups were found (*P* ≥ .05).

Quantitative Analysis

The intraclass correlation between the 2 independent readers was 0.984 with a 95% confidence interval of 0.982–0.985, indicating an excellent interreader reliability.

Attenuation

For the same CTDI_{vol}, attenuation in gray matter was significantly higher in VMI_{65keV} compared with CI (*P* ≤ .01 (Table 2). On the other hand, attenuation in white matter was slightly higher in CI compared with VMI_{65keV} for 55- and 49.8-mGy protocols without reaching a significant difference (*P* > .05), while for 44.7 mGy, it was slightly higher in VMI_{65keV} compared with CI (*P* > .05).

Noise

Image noise as indicated by an SD within the extraocular muscle was significantly lower in VMI_{65keV} compared with CI, irrespective of the CTDI_{vol} (*P* < .001 (Table 2 and Fig 2; eg, in 44.7-mGy protocol: 4.2 ± 1.6 versus 6.1 ± 2.1). Image noise slightly increased from 55 to 49.8 and 44.7 mGy, reaching a significant difference between 55- and 44.7-mGy protocols for the same reconstruction technique (eg, in CI: 5.3 ± 1.4 mGy versus 6.1 ± 2.1

mGy, $P = .004$). Yet, image noise in VMI_{65keV} with the 44.7-mGy protocol was significantly lower compared with CI and 55 mGy (4.2 ± 1.6 versus 5.3 ± 1.4 mGy, $P < .001$).

CNR

Overall, the CNR for gray-white matter differentiation was significantly higher in VMI_{65keV} compared with CI, irrespective of CTDI_{vol} ($P < .001$) (Table 2 and Fig 3). In line with noise, the CNR slightly decreased from 55 to 49.8 and 44.7 mGy, reaching a significant difference between 55- and 44.7-mGy protocols regarding the same reconstruction technique (eg, in VMI_{65keV}:

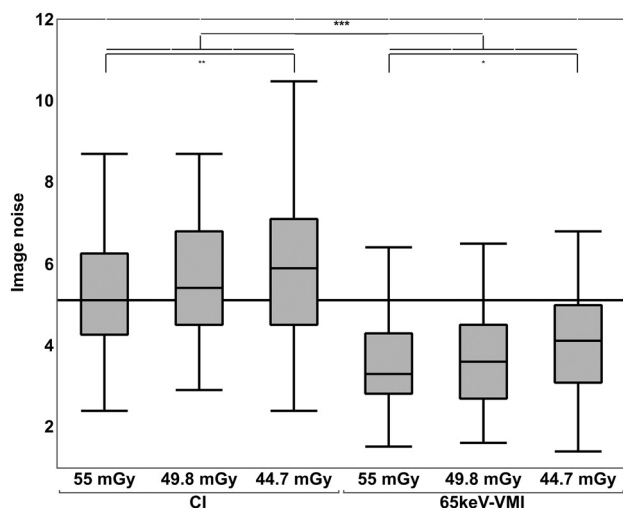


FIG 2. Image noise in extraocular muscle in CI compared with 65-keV virtual monoenergetic images regarding different radiation dose protocols. Significant differences are indicated. The asterisk indicates $P = .02$; double asterisks, $P = .004$; triple asterisks, $P < .001$.

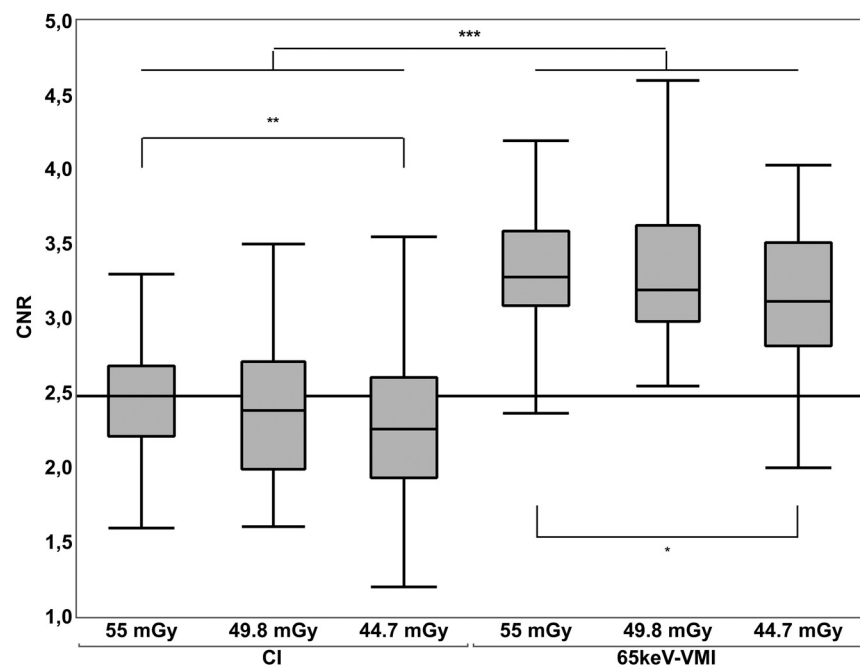


FIG 3. The CNR of gray-white matter differentiation in CI compared with 65-keV virtual monoenergetic images regarding different radiation dose protocols. Significant differences are indicated (asterisk, $P = .04$; double asterisks, $P = .02$; triple asterisks, $P < .001$).

3.4 ± 0.5 versus 3.2 ± 0.5 mGy, $P = .04$). Yet, the CNR in VMI_{65keV} with 44.7 mGy was higher compared with CI with 55 mGy (3.2 ± 0.5 versus 2.5 ± 0.5 mGy, $P < .001$).

Qualitative Analysis

The intraclass correlation between the 2 independent readers was 0.887, indicating an excellent interreader reliability.

VMI_{65keV} were rated better compared with CI for all criteria (Fig 4). Irrespective of the CTDI_{vol}, gray-white matter differentiation of the basal ganglia, supra- and infratentorial corticomedullary differentiation, subjective image noise, and beam-hardening artifacts caused by the skull received superior Likert scores in VMI_{65keV} compared with CI ($P < .001$, Table 3). In the assessment of the subcalvarial space, all VMI_{65keV} were rated as significantly better than CI ($P < .001$), except for VMI_{65keV} with 49.8 mGy compared with CI with 55 and 44.7 mGy ($P < .05$).

DISCUSSION

This study compared the image quality of 65-keV virtual monoenergetic images with conventional images from unenhanced spectral detector CT datasets of the head acquired with different radiation doses. We were able to show that improved image quality in VMI_{65keV} allows dose reduction in cranial CT.

Our study included a radiation dose reduction of 9.5% and 18.7% in terms of CTDI_{vol}. In VMI_{65keV}, we observed significantly higher attenuation in gray matter concerning the same radiation dose and no significant differences in white matter. Image noise, on the other hand, was significantly lower compared with CI, irrespective of the radiation dose. This reduction resulted in a significantly higher CNR for gray-white matter differentiation in VMI_{65keV}.

Hence, objective image-quality parameters were significantly better in VMI_{65keV} compared with CI, irrespective of CTDI_{vol}. Accordingly, subjective image analysis indicated superiority of VMI_{65keV} over CI with regard to the diagnostic assessment, except for the assessment of the subcalvarial space, which was not significantly superior in all different radiation doses.

Because unenhanced cranial CT is the imaging method of choice for patients with neurologic deficits and to diagnose neurocranial traumatic lesions, there is a need for excellent image quality.^{3,30} At the same time, the radiation dose has to be as low as reasonably achievable because sensitive tissues are exposed.^{10,11,13} The observed image-quality parameters are in accordance with a recent study in which the same scanner and comparable image-acquisition parameters were used.⁶ Compared with a study by Pomerantz et al¹⁵ using a

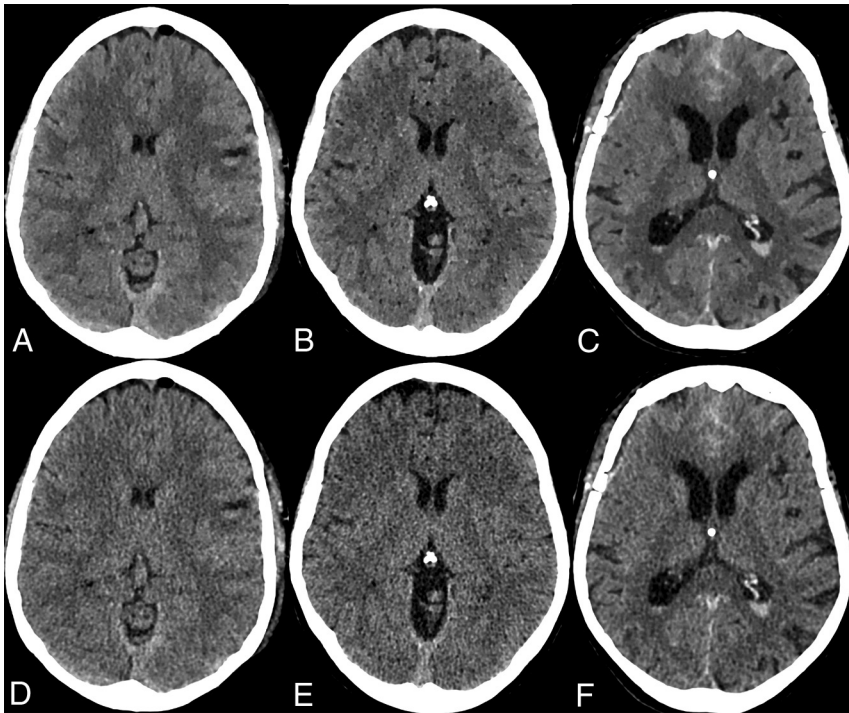


FIG 4. Examples of improved image quality in 65-keV virtual monoenergetic images acquired with a CTDI_{vol} with 55 mGy (A), 49.8 mGy (B), and 44.7 mGy (C) compared with CI, respectively (D–F).

Table 3: Qualitative results of subjective image parameters^a

CTDI _{vol} (mGy)	CI			VMI _{65keV}		
	55	49.8	44.7	55	49.8	44.7
GWMA	3 (3–3)	3 (3–3)	3 (3–3)	5 (5–5)	5 (5–5)	5 (4–5)
CMAS	3 (3–3)	3 (3–3)	3 (3–4)	5 (5–5)	5 (5–5)	5 (5–5)
CMAI	3 (3–3)	3 (3–3)	3 (2–3)	5 (5–5)	5 (5–5)	4 (4–5)
SSA	4 (4–5)	4 (4–4)	4 (4–5)	4 (4–5)	4 (4–5)	4 (4–5)
Noise	3 (3–3)	2 (2–3)	3 (3–3)	4 (4–4)	4 (4–4)	4 (4–4)
Artifacts	3 (3–4)	3 (2–3)	3 (2–3)	4 (4–5)	4 (4–5)	4 (4–4)

Note:—GWMA indicates assessment of gray-white matter differentiation of the basal ganglia; CMAS, assessment of corticomedullary differentiation supratentorially; CMAI, assessment of corticomedullary differentiation infratentorially; SSA, assessment of subcalvarial space.

^aResults are medians (quartiles).

kilovolt-switching dual-energy CT system with a CTDI_{vol} of 72.65 mGy, our CNR values are about 1.5 times higher and image noise is slightly lower. This result is likely due to advantages regarding image noise enabled by the detector-based approach.^{24,31} While we compared VMI_{65keV} with a state-of-the-art hybrid iterative reconstruction algorithm, whether most recent model-based image reconstructions can outperform noise reduction enabled by means of VMI remains elusive.³²

So far, only a few studies have investigated dose reduction in head imaging by means of VMI compared with polychromatic CT using a kilovolt-switching dual-energy CT system. Kamiya et al³³ included a radiation dose reduction of 11% in VMI_{65keV} compared with CI (CTDI_{vol}: 70.2 ± 0.3 mGy versus 78.9 ± 2.1 mGy), while maintaining comparable image quality. However, they reported significantly higher subjective image noise in VMI_{65keV}. On the contrary, besides an overall lower radiation dose in our study of 18.7%, we yielded superior image quality

quantitatively and qualitatively in VMI_{65keV}. In line with the study by Pomerantz et al,¹⁵ Kamiya et al³³ reported a lower CNR and higher noise as opposed to the results reported in this study. While the aforementioned results were reported for the supratentorial parenchyma only, we included a detailed analysis of the posterior fossa to address the most challenging region in cranial CT. Here, we report superior image quality in VMI_{65keV} compared with CI, even with a reduced radiation dose.

A more recent study by Hwang et al³⁴ investigated a radiation dose reduction of up to 37% compared with CI (CTDI_{vol} = 28.0 ± 0.9 mGy versus 44.1 ± 1.7 mGy) using VMI with different kiloelectron volt values in their analyses. Yet, they conducted only a subjective analysis of image quality, reporting no significant difference. In their study, subjective overall image noise was optimal in VMI from 60 to 70 keV, which is in accordance with a few prior studies investigating optimal kiloelectron volt values for VMI in cranial CT.^{6,15}

There are several limitations to this study. First, this was a retrospective study performed at a single institution. We were only able to include a limited number of patients because the radiation dose reduction was conducted in the run of the clinical routine; therefore, no prior power analysis was conducted. Thus, no greater reduction of the radiation dose could be evaluated,

though our data suggest that this is achievable. We compared the radiation dose based on the CTDI_{vol} alone because there is no established method to normalize radiation dose to the size of the head (unlike the size-specific dose estimates for body CT).^{35,36} Although our qualitative analysis was conducted in a blinded fashion, differences between CI and VMI_{65keV} are likely detectable by an experienced reader due to differences in image texture.^{32,37} Last, we quantitatively and qualitatively assessed image-quality parameters; however, an evaluation of diagnostic certainty and accuracy in pathologies was beyond the scope of this study.

CONCLUSIONS

The 65-keV virtual monoenergetic images from spectral detector CT enable a radiation dose reduction of 19% in cranial CT, while maintaining superior image quality over conventional images

from full-dose acquisitions. Our data further suggest that an even greater dose reduction seems achievable.

Disclosures: Jan Borggreffe—UNRELATED: Payment for Lectures Including Service on Speakers Bureaus: Philips Healthcare; Comments: I was paid 2 times for scientific lectures in 2017 and 2018. Nils Große Hokamp—UNRELATED: Grants/Grants Pending: Philips Healthcare*; Payment for Lectures Including Service on Speakers Bureaus: Philips Healthcare; Payment for Development of Educational Presentations: Philips Healthcare. *Money paid to institution.

REFERENCES

1. Chalela JA, Kidwell CS, Nentwich LM, et al. **Magnetic resonance imaging and computed tomography in emergency assessment of patients with suspected acute stroke: a prospective comparison.** *Lancet* 2007;369:293–98 [CrossRef Medline](#)
2. Farzad A, Radin B, Oh JS, et al. **Emergency diagnosis of subarachnoid hemorrhage: an evidence-based debate.** *J Emerg Med* 2013;44:1045–53 [CrossRef Medline](#)
3. Kim ES, Yoon DY, Lee HY, et al. **Comparison of emergency cranial CT interpretation between radiology residents and neuroradiologists: transverse versus three-dimensional images.** *Diagn Interv Radiology* 2014;20:277–84 [CrossRef Medline](#)
4. Hemphill JC, 3rd, Greenberg SM, Anderson CS, et al. **Guidelines for the Management of Spontaneous Intracerebral Hemorrhage: A Guideline for Healthcare Professionals from the American Heart Association/American Stroke Association.** *Stroke* 2015;46:2032–60 [CrossRef Medline](#)
5. Brenner DJ. **Slowing the increase in the population dose resulting from CT scans.** *Radiat Res* 2010;174:809–15 [CrossRef Medline](#)
6. Neuhaus V, Abdullayev N, Große Hokamp N, et al. **Improvement of image quality in unenhanced dual-layer CT of the head using virtual monoenergetic images compared with polyenergetic single-energy CT.** *Invest Radiol* 2017;52:470–76 [CrossRef Medline](#)
7. Liu X, Chen L, Qi W, et al. **Thin-slice brain CT with iterative model reconstruction algorithm for small lacunar lesions detection: image quality and diagnostic accuracy evaluation.** *Medicine (Baltimore)* 2017;96:e9412 [CrossRef Medline](#)
8. Lennartz S, Laukamp KR, Neuhaus V, et al. **Dual-layer detector CT of the head: Initial experience in visualization of intracranial hemorrhage and hypodense brain lesions using virtual monoenergetic images.** *Eur J Radiol* 2018;108:177–83 [CrossRef Medline](#)
9. Neverauskiene A, Maciusovic M, Burkanas M, et al. **Image based simulation of the low dose computed tomography images suggests 13 mAs 120kV suitability for non-syndromic craniosynostosis diagnosis without iterative reconstruction algorithms.** *Eur J Radiol* 2018;105:168–74 [CrossRef Medline](#)
10. Stewart FA, Akleyev AV, Akleyev AV, et al; Authors on Behalf of ICRP. **ICRP publication 118: ICRP statement on tissue reactions and early and late effects of radiation in normal tissues and organs—threshold doses for tissue reactions in a radiation protection context.** *Ann ICRP* 2012;41:1–322 [CrossRef Medline](#)
11. Sanchez RM, Vano E, Fernandez JM, et al. **Brain radiation doses to patients in an interventional neuroradiology laboratory.** *AJNR Am J Neuroradiol* 2014;35:1276–80 [CrossRef Medline](#)
12. Guzinski M, Waszczuk L, Sasiadek MJ. **Head CT: image quality improvement of posterior fossa and radiation dose reduction with ASiR—comparative studies of CT head examinations.** *Eur Radiol* 2016;26:3691–96 [CrossRef Medline](#)
13. Guberina N, Forsting M, Ringelstein A. **Efficacy of lens protection systems: dependency on different cranial CT scans in the acute stroke setting.** *Radiat Prot Dosimetry* 2017;175:279–83 [CrossRef Medline](#)
14. Silva AC, Morse BG, Hara AK, et al. **Dual-energy (spectral) CT: applications in abdominal imaging.** *Radiographics* 2011;31:1031–1046 discussion 1047–50 [CrossRef Medline](#)
15. Pomerantz SR, Kamalian S, Zhang D, et al. **Virtual monochromatic reconstruction of dual-energy unenhanced head CT at 65-75 keV maximizes image quality compared with conventional polychromatic CT.** *Radiology* 2013;266:318–25 [CrossRef Medline](#)
16. Schneider D, Apfaltrer P, Sudarski S, et al. **Optimization of kiloelectron volt settings in and cervical dual-energy CT angiography determined with virtual monoenergetic imaging.** *Acad Radiol* 2014;21:431–36 [CrossRef Medline](#)
17. Tawfik AM, Kerl JM, Razek AA, et al. **Image quality and radiation dose of dual-energy CT of the head and neck compared with a standard 120-kVp acquisition.** *AJNR Am J* 2011;32:1994–99 [CrossRef Medline](#)
18. Bodanapally UK, Dreizin D, Issa G, et al. **Dual-energy CT in enhancing subdural effusions that masquerade as subdural hematomas: diagnosis with virtual high-monochromatic (190-keV) images.** *AJNR Am J Neuroradiol* 2017;38:1946–52 [CrossRef Medline](#)
19. Van Hedent S, Große Hokamp N, Laukamp KR, et al. **Differentiation of hemorrhage from iodine using spectral detector CT: a phantom study.** *AJNR Am J Neuroradiol* 2018;39:2205–10 [CrossRef Medline](#)
20. Kaemmerer N, Brand M, Hammon M, et al. **Dual-energy computed tomography angiography of the head and neck with single-source computed tomography: a new technical (split filter) approach for bone removal.** *Invest Radiol* 2016;51:618–23 [CrossRef Medline](#)
21. Mannil M, Ramachandran J, Vittoria de Martini I, et al. **Modified dual-energy algorithm for calcified plaque removal: evaluation in carotid computed tomography angiography and comparison with digital subtraction angiography.** *Invest Radiol* 2017;52:680–85 [CrossRef Medline](#)
22. Borggreffe J, Kottlors J, Mirza M, et al. **Diffrentiation of clot composition using conventional and dual-energy computed tomography.** *Clin Neurodiol* 2018;4:515–22 [CrossRef Medline](#)
23. Alvarez RE, Macovski A. **Energy-selective reconstructions in X-ray computerized.** *Phys Med Biol* 1976;21:733–44 [CrossRef Medline](#)
24. Große Hokamp N, Höink AJ, Doerner J, et al. **Assessment of arterially hyper-enhancing liver lesions using virtual monoenergetic images from spectral detector CT: phantom and patient experience.** *Abdom Radiol (NY)* 2018;43:2066–74 [CrossRef Medline](#)
25. Flohr TG, McCollough CH, Bruder H, et al. **First performance evaluation of a dual-source CT (DSCT) system.** *Eur Radiol* 2006;16:256–68 [CrossRef Medline](#)
26. McCollough CH, Leng S, Yu L, et al. **Dual- and multi-energy CT: principles, technical approaches, and clinical applications.** *Radiology* 2015;276:637–53 [CrossRef Medline](#)
27. Gamer M, Lemon J, Fellows I, et al. **Package irr: various coefficients of interrater reliability and agreement.** 2012. <https://CRAN.R-project.org/package.org/package-irr>. Accessed March 25, 2019
28. Cohen J. **A coefficient of agreement for nominal scales.** *Educational and Psychological Measurement* 1960;20:37–46 [CrossRef](#)
29. Fleiss JL, Cohen J. **The equivalence of weighted kappa and the intraclass correlation coefficient as measures of reliability.** *Educational and Psychological Measurement* 1973;33:613–19 [CrossRef](#)
30. Smits M, Dippel DW, de Haan GG, et al. **External validation of the Canadian CT Head Rule and the New Orleans Criteria for CT scanning in patients with minor head injury.** *JAMA* 2005;294:1519–25 [CrossRef Medline](#)
31. Große Hokamp N, Hellerbach A, Gierich A, et al. **Reduction of artifacts caused by deep brain stimulating electrodes in cranial computed tomography imaging by means of virtual monoenergetic images, metal artifact reduction algorithms, and their combination.** *Invest Radiol* 2018;53:424–31 [CrossRef Medline](#)
32. Große Hokamp N, Gilkeson R, Jordan MK, et al. **Virtual monoenergetic images from spectral detector CT as a surrogate for conventional CT images: unaltered attenuation characteristics with reduced image noise.** *Eur J Radiol* 2019;117:49–55 [CrossRef Medline](#)
33. Kamiya K, Kunimatsu A, Mori H, et al. **Preliminary report on virtual monochromatic spectral imaging with fast kVp switching dual energy head CT: comparable image quality to that of 120-kVp CT**

- without increasing the radiation dose. *Jpn J Radiol* 2013;31:293–98 [CrossRef Medline](#)
34. Hwang WD, Mossa-Basha M, Andre JB, et al. **Qualitative comparison of noncontrast head dual-energy computed tomography using rapid voltage switching technique and conventional computed tomography.** *J Comput Assist Tomogr* 2016;40:320–25 [CrossRef Medline](#)
35. American Association of Physicists in Medicine (TaskGroup204). **Size-specific dose estimates (SSDE) in pediatric and adult body CT examinations.** 2011. <https://www.aapm.org/pubs/reports/detail.asp?docid=143>. Accessed April 12, 2019
36. McMillan K, Bostani M, Cagnon C, et al. **Size-specific, scanner-independent organ dose estimates in contiguous axial and helical head CT examinations.** *Med Phys* 2014;41:121909 [CrossRef Medline](#)
37. Kalisz K, Rassouli N, Dhanantwari A, et al. **Noise characteristics of virtual monoenergetic images from a novel detector-based spectral CT scanner.** *Eur J Radiol* 2018;98:118–25 [CrossRef Medline](#)